
Research Article: New Research | Neuronal Excitability

Medial Ganglionic Eminence Progenitors Transplanted into Hippocampus Integrate in a Functional and Subtype-Appropriate Manner

Optogenetic MGE Transplantation

Jui-Yi Hsieh and Scott C. Baraban

Epilepsy Research Laboratory, Department of Neurological Surgery, and Weill Institute of Neurosciences, University of California, San Francisco, California 94143

DOI: 10.1523/ENEURO.0359-16.2017

Received: 7 December 2016

Revised: 22 March 2017

Accepted: 4 April 2017

Published: 6 April 2017

Author contributions: J.-Y.H. and S.C.B. designed research; J.-Y.H. performed research; J.-Y.H. analyzed data; J.-Y.H. and S.C.B. wrote the paper.

Funding: HHS | NIH | National Institute of Neurological Disorders and Stroke (NINDS)
100000065
R37-NS071785

Conflict of Interest: Authors report no conflict of interest.

This work was supported, in part, by National Institute of Neurological Disorders and Stroke Grant R37-NS071785 (to S. C. Baraban).

Corresponding author: Jui-Yi Hsieh, 513 Parnassus Ave, Health Science East 840, San Francisco CA 94143, E-mail: Jui-yi.Hsieh@ucsf.edu

Cite as: eNeuro 2017; 10.1523/ENEURO.0359-16.2017

Alerts: Sign up at eneuro.org/alerts to receive customized email alerts when the fully formatted version of this article is published.

Accepted manuscripts are peer-reviewed but have not been through the copyediting, formatting, or proofreading process.

This is an open-access article distributed under the terms of the Creative Commons Attribution 4.0 International (<http://creativecommons.org/licenses/by/4.0>), which permits unrestricted use, distribution and reproduction in any medium provided that the original work is properly attributed.

Copyright © 2017 the authors

- 1 Title: Medial Ganglionic Eminence Progenitors Transplanted into Hippocampus Integrate in a
- 2 Functional and Subtype-Appropriate Manner
- 3 Abbreviated title: Optogenetic MGE Transplantation
- 4 Authors: Jui-Yi Hsieh and Scott C. Baraban
- 5 Author affiliation: Epilepsy Research Laboratory in the Department of Neurological Surgery and
- 6 Weill Institute of Neurosciences, University of California, San Francisco, California 94143
- 7 Corresponding author: Jui-Yi Hsieh; Jui-Yi.Hsieh@ucsf.edu; 513 Parnassus Ave, Health Science
- 8 East 840, San Francisco CA 94143
- 9 Number of pages: 38
- 10 Number of figures: 8
- 11 Number of words for Abstract: 171
- 12 Number of words for Significance statement: 96
- 13 Number of words for Introduction: 621
- 14 Number of words for Discussion: 1447
- 15 Conflict of interest: The authors declare no competing financial interests.
- 16 Acknowledgements: This work was supported, in part, by National Institute of Neurological
- 17 Disorders and Stroke Grant R37-NS071785 (to S. C. Baraban)

Abstract

19

20 Medial ganglionic eminence (MGE) transplantation rescues disease phenotypes in various
21 preclinical models with interneuron deficiency or dysfunction, including epilepsy. While
22 underlying mechanism(s) remains unclear to date, a simple explanation is that appropriate
23 synaptic integration of MGE-derived interneurons elevates GABA-mediated inhibition, and
24 modifies the firing activity of excitatory neurons in the host brain. However, given the
25 complexity of interneurons and potential for transplant-derived interneurons to integrate or alter
26 the host network in unexpected ways, it remains unexplored whether synaptic connections
27 formed by transplant-derived interneurons safely mirror those associated with endogenous
28 interneurons. Here, we combined optogenetics, interneuron-specific Cre driver mouse lines, and
29 electrophysiology to study synaptic integration of MGE progenitors. We demonstrated that
30 MGE-derived interneurons, when transplanted into the hippocampus of neonatal mice, migrate in
31 the host brain, differentiate to mature inhibitory interneurons, and form appropriate synaptic
32 connections with native pyramidal neurons. Endogenous and transplant-derived MGE
33 progenitors preferentially formed inhibitory synaptic connections onto pyramidal neurons but not
34 endogenous interneurons. These findings demonstrate that transplanted MGE progenitors
35 functionally integrate into the postnatal hippocampal network.

36

Significance Statement

38 We found that transplanted MGE-derived interneurons functionally innervate host neurons in a
39 manner similar to interneurons derived from endogenous MGE. Developmental lineage,
40 innervation preference and synaptic kinetics are similar. We also found that the transplanted

interneurons generate a passive inhibition on the firing activity of native pyramidal cells but not local interneurons. This inhibition only shifts but does not narrow the dynamic range of spiking suggesting the protective effect does not interfere with normal circuit function. Together, our findings suggest that transplanted MGE-derived interneurons interact with and function in host circuits in ways mirroring native interneurons.

Introduction

Interneuron-based cell therapy holds the potential to modify neural networks and ameliorate disease states. In recent studies, transplantation of interneuron progenitors from mouse embryonic medial ganglionic eminence (MGE) has been shown to be beneficial in various preclinical disease models, including epilepsy, associated with interneuron deficiency or dysfunction (Baraban et al., 2009; Hunt et al., 2013; Perez and Lodge, 2013; Tong et al., 2014; Tyson and Anderson, 2014). The premise underlying the success of these transplantations is that embryonic MGE progenitors are programmed to become GABAergic interneurons and specifically, parvalbumin- and somatostatin-positive interneurons (Anderson et al., 1997; Wichterle et al., 2001). Because PV⁺ and SST⁺ interneurons are strategically positioned to control network excitability, the beneficial effects of MGE transplantation are attributed to the functional synaptic integration of these transplant-derived inhibitory interneurons in the host brain. In support of this hypothesis (i) current-clamp recordings from transplant-derived cells confirm their integration as interneurons with mature firing properties, (ii) voltage-clamp recordings from host pyramidal neurons in brain regions containing transplant-derived interneurons indicate a significant increase in inhibitory postsynaptic current and (iii) electron

64 microscopy in tissue from transplanted brains shows the formation of new synaptic connections
65 between transplant-derived and host neurons (Alvarez-Dolado et al., 2006; Baraban et al., 2009;
66 Calcagnotto et al., 2010; Howard et al., 2014; Southwell et al., 2014; Hunt and Baraban, 2015).
67 While these studies are consistent with the idea that MGE progenitors are destined to integrate as
68 inhibitory interneurons, they do not directly evaluate functional synaptic connectivity between
69 transplant-derived interneurons and native neurons in the host brain.

70

71 To evaluate synaptic integration, it is necessary to directly study connections made between
72 interneurons and principal cells. As mentioned, MGE progenitor cells mostly differentiate into
73 fast-spiking PV⁺ and regular-spiking non-pyramidal SST⁺ interneurons (Wichterle et al., 2001;
74 Xu et al., 2004; Butt et al., 2005; Du et al., 2008; reviewed by Kepecs and Fishell, 2014). We
75 and other researchers have reported that the majority of transplanted MGE progenitor cells also
76 derives into PV⁺ and SST⁺ interneurons regardless of the brain regions they are grafted into, and
77 that they receive excitatory input and show intrinsic properties similar to native interneurons of
78 the same subtype (Alvarez-Dolado et al. 2006; Hunt et al., 2013; Hunt and Baraban, 2015;
79 Hammad et al., 2015; Zhou et al., 2015; Howard and Baraban, 2016). It is widely accepted that
80 endogenous PV⁺ interneurons primarily form fast and synapses around the somatic regions of
81 pyramidal cells, whereas endogenous SST⁺ cells mainly form slower inputs in the dendritic
82 regions (Lee et al., 2013; Pfeffer et al., 2013). Although interneuron identities are largely
83 controlled by the molecular programs established in the progenitor cells, whether transplant-
84 derived PV⁺ and SST⁺ interneurons innervate postsynaptic targets and exhibit functional synaptic
85 properties similar to their endogenous counterparts are yet to be firmly established.

86

87 To address these two issues, we investigated postsynaptic targets of MGE-derived progenitors
88 transplanted into hippocampal networks. This was possible because of recent advances in
89 optogenetics and establishment of interneuron-specific Cre mice, including GAD2-IRES-Cre,
90 PV-Cre and SST-IRES-Cre lines. These tools provide a powerful method for conditional
91 expression of channelrhodopsin 2 (ChR2) in interneuron subpopulations and for selective
92 stimulation of those subpopulations. MGE progenitor cells were harvested from donor mice
93 expressing ChR2 and transplanted into the hippocampus of recipient wild-type pups. These
94 ChR2-carrying MGE progenitor cells, depending on their genotype, are referred to here as
95 GAD2-ChR2 MGE, PV-ChR2 MGE, and SST-ChR2 MGE, respectively. A schematic
96 illustration of the experimental protocol is shown in Figure 1A. We employed whole-cell patch-
97 clamp electrophysiology and optogenetic manipulations to identify synaptic targets of
98 transplanted interneurons, and analyzed synaptic properties. We found that transplanted MGE-
99 derived interneurons not only show similar selectivity in innervation as native interneurons, but
100 also generate postsynaptic currents with characteristics corresponding to their subtypes.

101

102 **Materials and Methods**

103

104 **Animals and tissue transplantation**

105

106 All procedures and protocols were approved by the Institutional Animal Care and Use
107 Committee at University of California, San Francisco (Protocol#: AN151703). Mice were
108 maintained under standard conditions with 12-hr day/dark cycle, and both male and female mice
109 were used in this study indiscriminately.

110

111 Medial ganglionic eminence (MGE) transplantation was performed as previously described
112 (Cobos et al., 2005; Alvarez-Dolado et al., 2006; Baraban et al., 2009). Briefly, MGE progenitor
113 cells were harvested from donor embryos (E12.5-E14.5) and mechanically dissociated by
114 pipetting in Leibovitz L-15 medium (UCSF, Cell Culture Facility) containing 1% DNase
115 (Qiagen). Cells were concentrated by centrifugation and front loaded into beveled glass needles
116 with openings between 60-80 μ m. Stereotaxic injections into dorsal hippocampi were performed
117 bilaterally in neonatal pups (postnatal day 1 to 4) anesthetized with ice (Figure 1A) to minimize
118 the number of animals required to complete these studies. Wild-type CD1 (Charles River) mice
119 were used as recipients to transplantation. A ChR2-eYFP line (Jackson Lab, #012569, aka Ai32)
120 was crossed with various Cre lines to generate ChR2-positive embryos, including Gad2-IRES-
121 Cre (Jackson Lab, #010802), Parv-Cre (Jackson Lab, #008069) and Sst-IRES-Cre (Jackson Lab,
122 #013044). These embryos served as MGE progenitor cell donors. It is important to note that the
123 Cre-Lox system was employed only to control the subpopulation of cells expressing ChR2 and
124 not the type of cells transplanted. In some experiments, offspring of these ChR2-expressing
125 mice were used as control animals in electrophysiological experiments between P30-P70.

126

127 **Immunohistochemistry**

128

129 Wild-type CD1 mice transplanted with MGE progenitor cells harvested from Gad2-IRES-
130 Cre;Ai32 embryos were transcardially perfused with 4% paraformaldehyde (vol/vol in PBS)
131 between 28-70 days after transplantation (DAT). Brains were coronally sectioned at 50 μ m
132 using a vibratome (Leica VT 1000S). Sections were labeled using the following primary

133 antibodies: chicken anti-GFP (Aves, GFP-1020 at 1:500) for ChR2-eYFP, mouse anti-
134 parvalbumin (Sigma, P3088 at 1:500) for parvalbumin (PV), and goat anti-somatostatin (Santa
135 Cruz, sc-7819 at 1:200) for somatostatin (SST). Secondary antibodies (all from Thermo Fisher)
136 used were anti-chicken Alexa Fluor 488, anti-mouse Alexa Fluor 594, and anti-goat Alexa Fluor
137 594. Labeled fluorescent cells were visualized under an upright microscope (Nikon) and images
138 were captured by a CCD camera (Andor) and NIS-elements software (Nikon).

139

140 **Electrophysiology and optogenetic stimulation**

141

142 Mice were deeply anesthetized and decapitated. Brains were dissected out and sectioned at 300
143 μm along the coronal plane in ice-cold high-sucrose solution (in mM): 150 sucrose, 50 NaCl, 25
144 NaHCO_3 , 10 dextrose, 2.5 KCl, 1 $\text{NaH}_2\text{PO}_4\text{-H}_2\text{O}$, 0.5 CaCl_2 , 7 $\text{MgSO}_4\text{-7H}_2\text{O}$. Slices were then
145 transferred to regular artificial cerebrospinal fluid (aCSF, in mM): 124 NaCl, 3 KCl, 1.25
146 $\text{NaH}_2\text{PO}_4\text{-H}_2\text{O}$, 26 NaHCO_3 , 10 dextrose, 2 CaCl_2 , 2 $\text{MgSO}_4\text{-7H}_2\text{O}$, and incubated at 35°C for 30
147 min. A 45-min recovery time at room temperature was allowed before electrophysiological
148 recording were commenced. Kynurenic acid (3 mM) was added to the aCSF in all experiments to
149 block postsynaptic glutamate receptors.

150

151 ChR2-eYFP positive MGE-derived cells were identified in acute brain slices under an upright
152 fluorescence microscope (Olympus). Whole-cell patch-clamp was performed in the CA1 region
153 of hippocampi using 3-5 $\text{M}\Omega$ borosilicate electrodes on native pyramidal cells, native
154 interneurons, or transplanted interneurons. For voltage-clamp experiments, electrodes were filled
155 with high-chloride based internal solution (in mM): 140 CsCl, 1 MgCl_2 , 10 HEPES, 11 EGTA, 2

156 Mg-ATP, 0.5 Na-GTP. Cells were held at either -50 or -60 mV in all voltage-clamp
157 experiments. For current-clamp experiments, electrodes were filled with potassium-gluconate
158 based internal solution (in mM): 140 K-gluconate, 10 HEPES, 1 NaCl, 1 MgCl₂, 1 CaCl₂, 5
159 EGTA, 2 Mg-ATP, 0.2 Na-GTP. To eliminate possible complications caused by variations in
160 resting membrane potential, cells were held at -65 mV by injecting a small amount of current.
161 This holding current is defined as “baseline”, and all current injections in current-clamp
162 experiments are measured relative to this baseline. All recordings were acquired using an Axon
163 200B amplifier, Digidata 1550A digitizer and Clampex 10.5 software (all from Molecular
164 Device). Traces were sampled at 20 kHz and filtered at 5 kHz. Series resistance was monitored
165 but not compensated, and cells with series resistance greater than 20 MΩ were discarded.

166

167 A mercury lamp was used as the light source for optogenetic stimulation. A GFP and a RFP filter
168 cube were used to isolate blue and green light, respectively. The diameter of illumination was ~2
169 mm under a 40X water-immersion objective lens, and the intensity was 1 to 2.3 mW/mm²
170 measured by a power meter (ThorLabs). Optogenetic stimulation was time-locked with
171 electrophysiological recordings through the Digidata 1500A digitizer. The light pulse was set at
172 10 ms and controlled by an in-line shutter system (Uniblitz) in all experiments.

173

174 **Data analysis**

175

176 Fluorescence images from immunostaining experiments were analyzed with NIS-elements
177 software (Nikon), and co-localization of green and red fluorescent signal was identified in the
178 software. Numbers of transplanted cells and co-labeled cells were counted manually.

179 Electrophysiological data were analyzed with Clampfit 10.5 software (Molecular Device) and
180 Microsoft Excel (Microsoft). Data are provided as mean \pm SEM. Statistical significance was
181 assessed in OriginPro 2016 software (OriginLab). All figures were prepared in OriginPro 2016
182 and Adobe Illustrator (Adobe).

183

184 **Results**

185

186 **Transplanted MGE-derived cells integrate as parvalbumin- and somatostatin-positive** 187 **interneurons**

188

189 In rodents, transplanted embryonic MGE progenitors maintain a unique ability to migrate widely
190 in the host brain where they differentiate into parvalbumin-positive (PV⁺) and somatostatin-
191 positive (SST⁺) interneurons (Wichterle et al. 1999; Butt et al., 2005; Alvarez-Dolado et al.
192 2006; Fogarty et al., 2007; Du et al., 2008; Hunt et al., 2013; Howard et al., 2014; Kepecs and
193 Fishell, 2014; Hunt and Baraban, 2015). To confirm the developmental lineage of our
194 anatomically isolated MGE progenitor cells, brains transplanted with GAD2-ChR2 MGE were
195 stained for ChR2-eYFP, PV, and SST at 28-70 days after transplantation (DAT). Many of the
196 transplanted ChR2-eYFP⁺ cells co-labeled for PV (Figure 1B) or SST (Figure 1C). Quantitative
197 analysis showed that $28.8 \pm 1.9\%$ of the MGE-derived ChR2-eYFP⁺ cells were also PV⁺, and
198 $36.3 \pm 1.9\%$ were SST⁺ (Figure 1D). These results using ChR2 mouse donor embryos are
199 consistent with previous studies (Alvarez-Dolado et al., 2006; Baraban et al., 2009; Southwell et
200 al., 2012; Sebe et al., 2014a; Sebe et al., 2014b; Hunt et al., 2013; Howard et al., 2014; Hunt and
201 Baraban, 2015; Howard and Baraban, 2016)

202

203 **MGE-derived interneurons increase inhibition by forming functional inhibitory synapses**
204 **with native neurons**

205

206 In regions of cortex or hippocampus containing MGE-derived interneurons, inhibitory
207 postsynaptic currents (IPSCs) measured on host pyramidal neurons are increased by 20-40%
208 compared to controls starting at 30 DAT (Calcagnotto et al., 2005; Alvarez-Dolado et al., 2006;
209 Baraban et al., 2009). To confirm an enhancement of inhibition using ChR2 expressing donors,
210 whole-cell voltage-clamp was performed on CA1 pyramidal cells in MGE transplanted and non-
211 transplanted mice between 30-70 DAT. As expected, mice with MGE-derived interneurons in
212 area CA1 exhibited a significantly higher frequency of spontaneous inhibitory postsynaptic
213 currents (IPSCs) compared to non-transplanted mice (Figure 2B). As an internal control, we also
214 recorded from pyramidal cells in transplanted mice that did not connect with exogenous ChR2-
215 expressing cells. They showed the same level of spontaneous IPSCs as those seen in non-
216 transplanted mice (Figure 2B). This observation strongly suggests the enhancement in inhibition
217 is a direct result of the exogenous MGE-derived interneurons rather than a non-specific effect.

218

219 A plausible and likely interpretation for the enhancement of GABA-mediated inhibition
220 consistently observed with MGE transplantation (Calcagnotto et al., 2005; Alvarez-Dolado et al.,
221 2006; Baraban et al., 2009; Figure 2) is that MGE-derived interneurons make functional
222 inhibitory synapses onto native pyramidal cells. To directly test this hypothesis, we used
223 optogenetics to photostimulate MGE-derived interneurons carrying ChR2, and then monitored
224 light-evoked responses in native pyramidal neurons or interneurons in area CA1. Brief 10 ms

225 blue-light pulses consistently elicit action potentials greater than 40 mV in amplitude on GAD2-
226 ChR2-expressing interneurons (n=4; Figure 3A). The number of action potentials (APs) evoked
227 varied slightly between cells, presumably associated with the differential excitability of
228 interneuron subtypes and cell-to-cell variability in the level of GAD2-ChR2 expression.
229 However, the number of APs evoked was consistent within the same cell. Light-evoked APs
230 were not sensitive to the addition of a GABA-receptor antagonist (100 μ M gabazine; Figure 3A).
231 Since we also included a non-specific glutamate receptor blocker (3 mM kynurenic acid) in the
232 aCSF for all recordings (see also Methods), these observations suggest that light-evoked
233 responses are intrinsic to the ChR2-expressing neurons. Brief 10 ms green-light pulses did not
234 generate action potentials (Figure 3A). When recording from native pyramidal cells, evoked
235 IPSCs ranged from 10.5 to 403.3 pA in amplitude (n = 11) and were consistently observed
236 immediately after blue-light pulses, whereas green-light pulses did not elicit responses (Figure
237 3B). All light-evoked IPSCs were eliminated by 100 μ M gabazine indicating a dependence on
238 GABA receptor-mediated synaptic inputs. Taken together, these findings suggest that
239 transplanted MGE-derived interneurons increase the level of inhibition in hippocampal circuits
240 by forming functional inhibitory synapses with native neurons.

241

242 Physiologically, MGE-derived interneurons primarily innervate neurons in stratum pyramidale
243 and stratum lacunosum moleculare, but not nearby interneurons in the stratum oriens (Elfant et
244 al., 2008; Lovett-Barron et al., 2012; Bezaire and Soltesz, 2013; Kepecs and Fishell, 2014).
245 GABA-mediated inhibition onto native interneurons in regions containing MGE-derived
246 interneurons was not found to be enhanced in cortex (Baraban et al. 2009). These findings are
247 consistent with our interpretation that MGE-derived interneurons selectively innervate native

pyramidal neurons following transplantation. To directly evaluate functional inhibitory connectivity between MGE-derived interneurons and host brain neurons, we also recorded from native interneurons in stratum oriens while optogenetically activating the MGE-derived GAD2-Chr2-expressing interneuron subpopulation. Photostimulation of MGE-derived interneurons did not consistently evoke IPSCs in native interneurons ($n = 16$; Figure 3C). Indeed, a light-evoked IPSC response was only observed on one native interneuron. As shown in Figure 3C, the amplitude of light-evoked events in this single interneuron were dramatically smaller (~ 15 pA) than those in Figure 3B (~ 80 pA) recorded from a native pyramidal cell. IPSC rising kinetics ($\tau = 16.3$ ms) of this interneuron was much slower than those observed in pyramidal cells (Figure 3B; see also Figure 4D and 5D). Thus, these results are also consistent with our hypothesis that MGE-derived interneurons primarily make functional inhibitory connections with native pyramidal neurons.

Transplanted and native interneurons share comparable IPSC kinetics in a cell-type specific manner

Endogenous parvalbumin fast-spiking interneurons primarily innervate somatic regions of pyramidal neurons and exhibit fast IPSC rise time kinetics, whereas somatostatin interneurons largely innervate dendrites and exhibit slower IPSC rising kinetics (Lee et al., 2013; Pfeffer et al., 2013). Whether exogenous MGE-derived PV^{+} and SST^{+} interneurons integrate in the host circuit in a similar manner is not known. To investigate the functional connections made by MGE-derived interneuron subpopulations, we generated MGE donors expressing Chr2-eYFP in either PV^{+} or SST^{+} cells for transplantation into recipient CD1 pups. This approach allowed us to

271 characterize the functional integration of MGE-derived interneuron sub-types in a cell-type
 272 specific manner. For control studies we used age-matched non-transplanted mice expressing
 273 ChR2-eYFP driven by PV- or SST-Cre promoters, Referred to here as native Parv-ChR2 (nParv-
 274 ChR2) and native SST-ChR2 (nSST-ChR2); transplanted PV⁺ and SST⁺ cells carrying ChR2-
 275 eYFP are referred to as tParv-ChR2 and tSST-ChR2, respectively. Photostimulation of nParv-
 276 ChR2 interneurons consistently generated large amplitude IPSCs in native pyramidal cells
 277 (ranged from 204.8 to 1817.1 pA, n = 10; Figure 4A). Light activation of tParv-ChR2 cells also
 278 evoked IPSC responses in native pyramidal cells but with smaller amplitudes (ranged from 19.1
 279 to 181.4 pA, n = 12), consistent with the presence of fewer MGE-derived PV⁺ interneurons
 280 (compared to native interneurons) in the host brain. A representative cell is shown in Figure 4B.
 281 Green-light pulses did not elicit IPSCs and 100 μ M gabazine eliminated both light-dependent
 282 and independent IPSCs. Despite the difference in amplitude, the rising kinetics of light-evoked
 283 IPSCs showed no differences between nParv-ChR2 and tParv-ChR2 cells. Both generated IPSCs
 284 with fast onset kinetics in pyramidal cells with a rising time constant of ~ 1.5 ms (1.6 ± 0.3 for
 285 nParv-ChR2, n = 12; 1.5 ± 0.1 for tParv-ChR2, n = 10; Figure 4D).
 286
 287 Next, we recorded postsynaptic responses of native pyramidal cells following photostimulation
 288 of nSST-ChR2 cells. A representative cell is shown in Figure 5A. Consistent IPSCs were
 289 observed immediately after blue-light pulses. The rising kinetics of these responses were smaller
 290 and slower than that from the nParv-ChR2 cell shown in Figure 4A ($\tau = 5.2$ for black trace in
 291 Figure 5A; $\tau = 1.8$ ms for black trace in Figure 4A). The amplitude of IPSCs from nSST-ChR2
 292 inputs ranges from 52.3 to 464.2 pA (n = 10), and the average time constant of rising was $6.8 \pm$
 293 0.9 ms, which is 4.3-times slower than the average from nParv-ChR2 at 1.6 ± 0.3 ms (Figure 4D)

294 and 5D). This finding is consistent with observations that PV⁺ interneurons generate faster
 295 postsynaptic currents in pyramidal cells than SST⁺ interneurons (Lee et al., 2013; Pfeffer et al.,
 296 2013). Activation of transplanted SST⁺ cells also generated consistent IPSCs in pyramidal cells,
 297 which could be blocked by subsequent addition of 100 μ M gabazine. IPSCs elicited by tSST-
 298 ChR2 cells have amplitudes ranging from 51.7 to 187.3 pA (n = 8), and their averaged time
 299 constant of rising is 5.7 ± 1.1 ms, which is not significantly different from that of nSST-ChR2
 300 (Figure 5D). Taken together, our results show that transplanted cells, either PV⁺ or SST⁺,
 301 generate subtype specific postsynaptic responses in pyramidal cells, mirroring those generated by
 302 native interneurons of the same subtype.

303

304 **Transplanted interneurons introduce inhibitory gain control to native pyramidal cells**
 305 **without altering their spiking behaviors**

306

307 To better understand the nature of inhibition introduced by transplantation and functional impact
 308 on local circuits, we generated current-frequency (I-F) curves for native pyramidal cells in
 309 regions containing MGE-derived GAD2-ChR2-expressing interneurons. Figure 6A shows
 310 representative recordings from a native pyramidal cell innervated by MGE-derived interneurons.
 311 In the absence of photostimulation, a 40-pA current injection elicited two action potentials giving
 312 a spiking frequency of 5 Hz; with 100-pA and 200-pA current injections, the frequencies elicited
 313 were 18.7 and 29.2 Hz respectively. With the presence of blue light stimulating the transplanted
 314 MGE-derived interneuron population, the same 40-pA current injection no longer generated any
 315 action potential in the recorded pyramidal cell (see red traces in Figure 6A). The spike frequency
 316 was lowered slightly at 100-pA current injection from 18.7 to 15.6 Hz, whereas that at 200-pA

317 injection stayed almost unaffected (29 Hz versus 28 Hz; Figure 6A). Further analysis showed
318 that photostimulation caused a right-shift in I-F curve of this cell, which could be reversed by the
319 addition of 100 μ M gabazine (Figure 6B-C). The I-F curves were fit with linear regression. The
320 data range used for fitting was selected manually for each neuron so that the r-squared value is
321 greater than 0.95 except in a few cases it was between 0.9 and 0.95. Slope factors and x-
322 intercepts (the axis for current injection) from the fitting results were analyzed and compared
323 between recording conditions: (i) with or without photostimulation, and (ii) with or without
324 gabazine. We found that on average photostimulating transplanted interneurons right-shifts the I-
325 F curve by 21.1 ± 5.5 pA without significantly affecting the slope factor ($n = 9$; Figure 6D-E).
326 The addition of gabazine completely blocked the effect, and reversed the shift to -2.2 ± 6.8 pA,
327 which is not significantly different from no-shift ($n = 5$, one sample t -test, $p = 0.661$).

328

329 To confirm that this parallel shift in I-F curve by exogenous interneurons is a physiological
330 function, we tested if native interneurons also showed a similar phenomenon. We repeated the
331 experiments and recorded from pyramidal cells in non-transplanted mice carrying ChR2 in all
332 interneurons (Gad2-IRES-Cre;Ai32). This allows us to investigate the connections formed
333 physiologically between native interneurons and pyramidal neurons. Photostimulation
334 significantly shifted the I-F curve to the right by 342.8 ± 30.3 pA ($n = 5$; Figure 6E) without
335 affecting the slope factors (data not shown). Again, this rightward shift could be reversed by the
336 addition of gabazine. Thus, transplanted MGE-derived interneurons appear to exert gain control
337 of pyramidal cell firing in a manner functionally similar to native interneurons.

338

339 To further identify the interneuron subtype-specific source of this inhibitory shift, we performed
340 current-clamp experiments on pyramidal cells while selectively activating either tParv-ChR2 or
341 tSST-ChR2 cells. We found that while 40-pA current injection was sufficient to bring a
342 pyramidal cell over action potential threshold, it failed to do so with simultaneous activation of
343 nearby tPV-ChR2 cells (Figure 7A). This effect was much less obvious when the level of current
344 injection was raised to 100-pA and 200-pA, with which the difference in spiking frequencies was
345 less than 5% with and without blue-light activation (19.7 and 17.7 Hz at 100-pA injection; 37.4
346 and 35.4 Hz at 200-pA injection; Figure 7A). By further analyzing the I-F curve, we found that
347 photostimulation shifted the curve to the right, and the addition of 100 μ M gabazine reversed the
348 effect (Figure 7B-C). We found that, on average, activating tParv-ChR2 cells right-shifts the I-F
349 curve of pyramidal cells by 12 ± 3.8 pA without significantly altering slope factors ($n = 8$), and
350 that this parallel shift can be completely eliminated by the addition of gabazine ($n = 6$; Figure
351 7D-E).

352
353 We next tested the functional impact of inhibition from tSST-ChR2 on pyramidal cells. Similar
354 to the examples shown earlier in this study, 40-pA current injection elicited an action potential in
355 a pyramidal cell, and simultaneous activation of tSST-ChR2 cells compromised this spike. This
356 suppression was nearly absent when the level of current injection was at 100-pA or 200-pA. The
357 impact on spiking frequency was very subtle if any (Figure 8A). The shift in I-F curve by
358 photostimulation was 9.1 pA in the cell shown in Figure 8A, and 100 μ M gabazine blocked the
359 shift completely (Figure 8B-C). The averaged right-shifts by photostimulation are 13.3 ± 5.2 pA
360 and 1.7 ± 2.6 pA without and with gabazine respectively (Figure 8E). The latter is not different
361 from zero (one-sample *t*-test, $n = 5$, $p = 0.513$) suggesting the expected indifference of I-F curve

362 to light in the presence of synaptic blocker, gabazine. Photostimulation did not change the slope
363 factor of I-F curves regardless the presence or absence of gabazine (Figure 8D). Our results
364 suggest that both transplanted PV⁺ and SST⁺ interneurons contribute to the introduction of gain
365 control following MGE transplantation.

366

367 **Discussion**

368

369 Inhibitory interneurons constitute about 20% of the neuronal population in cortical networks. In
370 general, interneuron synaptic interactions are short range and dense. Mature PV⁺ interneuron
371 axons target proximal dendrites and somata of pyramidal cells, close to where action potentials
372 are generated. Thus, their postsynaptic inhibitory effect is both powerful and precisely
373 coordinated. Mature SST⁺ interneurons are often dendritic-targeting and suppress dendritic
374 calcium spikes and bursting (Murayama et al., 2009), but have also been shown to modulate
375 pyramidal neuron firing (Lovett-Barron et al., 2012). These properties of interneurons derived
376 from MGE progenitors could explain the beneficial effects seen when embryonic MGE is
377 transplanted into various disease models associated with interneuron deficiency or dysfunction
378 (Baraban et al., 2009; Hunt et al., 2013; Perez and Lodge, 2013; Tong et al., 2014; Tyson and
379 Anderson, 2014). Indeed, the most parsimonious interpretation of these results coincides with a
380 concept first put forth by Prince and Wilder of an “inhibitory surround” (Prince and Wilder,
381 1967; Traub, 1983) near the seizure focus that constrains the spread of an epileptic discharge.
382 Theoretical calculations show that if the GABA-mediated inhibition is sufficiently powerful, it
383 can effectively suppress any amount of excitatory drive (Trevelyan and Watkinson, 2005).
384 However, other mechanisms explaining MGE transplantation have been put forth: (i)

385 reorganization of host circuitry by introducing a new set of weak inhibitory synapses (Southwell
386 et al., 2010; Southwell et al., 2014) or (ii) addition of “young” interneurons thus weakening
387 endogenous inhibition (Davis et al., 2015). Experimental support for transplanted MGE-derived
388 interneurons providing increased synaptic inhibition and enhanced inhibitory surround requires a
389 direct demonstration that these progenitors differentiate into mature PV⁺ and SST⁺ interneurons
390 making selective inhibitory synaptic connections within the host network. Using a combination
391 of *in vitro* electrophysiology and optogenetic techniques we provide that evidence here.

392

393 **Transplanted and endogenous MGE-derived interneurons share common synaptic targets**
394 **and physiology in a subtype-specific manner.**

395

396 For synaptic integration to be the working mechanism underlying a feasible cell-therapy, there
397 are three indispensable requirements: (i) the developmental lineage of transplanted MGE cells is
398 autonomous, (ii) the innervation targets of exogenous interneurons are inherently the same as
399 those of endogenous interneurons, and (iii) the synaptic physiology of exogenous interneurons
400 are comparable to that of endogenous interneurons. The first requirement is crucially important
401 because interneuron subtypes have distinct physiology and differential innervation preferences
402 that may provide opposite effects to local circuits. For instance, innervation on native pyramidal
403 cells offers inhibition, whereas that on native interneurons generates dis-inhibition, which
404 contradicts the goal of enhancing inhibitory surround. Interneuron complexity, however, raises
405 the possibility that transplant-derived interneurons could integrate in a random fashion with
406 inappropriate and detrimental consequences for circuit modification. Prior work suggests that
407 differentiation of transplanted embryonic MGE progenitors is autonomous (Butt et al., 2005;

408 Alvarez-Dolado et al. 2006; Fogarty et al., 2007; Du et al., 2008; Hunt et al., 2013; Howard et
409 al., 2014; Kepecs and Fishell, 2014; Hunt and Baraban, 2015; Howard and Baraban, 2016). Here,
410 we also found that transplanted MGE progenitors primarily derived into PV⁺ and SST⁺ cells
411 (Figure 1B-D), and formed functional synapses with host neurons (Figure 2).

412

413 As a means to control or modulate network excitability, the primary innervation targets for
414 endogenous MGE-derived interneurons are excitatory pyramidal neurons (Elfant et al., 2008;
415 Lovett-Barron et al., 2012; Bezaire and Soltesz, 2013; Kepecs and Fishell, 2014). It is important
416 that transplanted interneurons maintain this signature attribute and do not reorganize the host
417 network or target nearby native interneurons. Baraban et al. (2009) demonstrated there was no
418 elevation in spontaneous IPSC frequency onto native interneurons following transplantation into
419 cortex. Here, we employed optogenetic tools to more carefully evaluate potential connections
420 between transplant-derived and native interneurons. Compared to the previous study, this
421 approach is more sensitive because the transplanted ChR2-expressing interneurons were directly
422 activated to elicit measurable postsynaptic responses. Consistent with Baraban et al. (2009), we
423 found that native pyramidal neurons showed robust and gabazine-sensitive IPSCs (Figure 3) in
424 response to activation of transplanted interneurons. Among all the native interneurons recorded,
425 only one was found to connect with transplant-derived interneurons, and the response was very
426 small (see also Results). The rarity of this type of connection is consistent with the interpretation
427 that MGE-derived interneurons do not innervate other interneurons and preferentially make
428 connections with pyramidal cells. It is also possible a very small number of transplant-derived
429 interneurons arise from the caudal ganglionic eminence (CGE, a region generating interneuron-
430 innervating interneurons; Nery et al., 2002; Xu et al., 2004; Butt et al., 2005; Cobos et al., 2005;

431 Miyoshi et al., 2010; Kepecs and Fishell, 2014) as these are anatomical embryonic sub-
432 dissections and could include a small piece of CGE tissue. Furthermore, the fact that transplant-
433 derived and native interneurons share common geographic area and yet form virtually no
434 synapses argues against the idea that exogenous interneurons reorganize the host network and
435 provide non-specific inhibition to their immediate surroundings. Taken together, our data
436 strongly suggest that transplanted interneurons show an inherent innervation preference
437 mimicking endogenous MGE-derived interneurons.

438

439 Although we and several studies have reported that MGE-derived interneurons show comparable
440 intrinsic properties to endogenous interneurons following transplantation (Figure 1D-E; Alvarez-
441 Dolado et al. 2006; Hunt et al., 2013; Howard et al., 2014; Sebe et al., 2014b; Zhou et al., 2015),
442 it is not yet settled whether they also have proper synaptic characteristics matching their
443 interneuron subtypes. Comprehensive recapitulation of functional features is essential to any type
444 of cell-based therapy. Either gain-of-function or loss-of-function may lead to unwanted effects.
445 Recently, Howard and Baraban (2016) presented a detailed functional comparison between
446 transplant-derived and native PV⁺ interneurons. By performing dual whole-cell patch-clamp
447 from PV⁺ and pyramidal cells, they reported that in mouse cortex transplanted PV⁺ interneurons
448 (7-35 DAT) showed delayed but identical characteristics as native PV⁺ cells during maturation,
449 including their intrinsic properties, excitatory synaptic inputs, and post-synaptic properties. Here,
450 however, we focused on a functional comparison after transplanted neurons are mature (30-70
451 DAT), and we took one step further to distinguish both PV⁺ and SST⁺ cells. We found that MGE
452 transplant-derived interneurons formed appropriate connections with postsynaptic targets
453 matching their native interneuron subtypes in hippocampus e.g., PV⁺ cells generated fast IPSCs

454 on pyramidal cells and SST⁺ cells generated slow IPSCs. More importantly, kinetic properties of
455 these postsynaptic currents were comparable to that from native interneurons of the same
456 subtype (Figure 4-5). These findings extend and confirm our previous PV⁺ interneuron study
457 (Howard and Baraban, 2016). Taken together, we conclude that transplant-derived and
458 endogenous MGE-derived interneurons are fundamentally the same, sharing a common
459 developmental lineage, innervation preference, and synaptic function.

460

461 **Inhibitory gain-control generated by transplanted interneurons sheds light on the**
462 **feasibility of interneuron-based therapy.**

463

464 Here, we also investigated how MGE transplant-derived interneurons affect outputs of local
465 circuits e.g., the spiking behavior of pyramidal cells. Interactions between synaptic excitation
466 and inhibition are often presented in terms of a neuronal input-output function, also referred to as
467 “gain control” (reviewed by Silver, 2010 and by Trevelyan et al., 2015). Two different patterns
468 of inhibition underlie this gain control, and are provided by distinct interneuron subtypes that
469 target peripheral dendrites (SST⁺) or proximal dendrites and soma (PV⁺), respectively. These are
470 the same two interneuron subtypes generated from our MGE progenitor transplantations and we
471 demonstrated that they shift the frequency-current curve (I-F curve) to the right providing an
472 inhibitory gain control to endogenous pyramidal neurons (Figure 6E, 7E and 8E). This
473 phenomenon was not a gain-of-function effect because a similar but greater right-shift was also
474 found when we activated native interneurons (Figure 6E). The difference in magnitude of the I-F
475 shift is likely a reflection of a discrepancy in cell numbers. That is, the number of native
476 interneurons in a given hippocampal slice is significantly larger than that of transplant-derived

477 interneurons (Figure 1B-C). In either case, I-F curve was right-shifted in a parallel manner
478 suggesting that the introduced gain control primarily exerts its function in the sub-threshold
479 range and once the threshold is overcome, spiking behavior is solely determined by properties
480 intrinsic to the host circuits. For this reason, while the inhibitory gain control offers protective
481 effects during hyperexcitable network disease states such as during a seizure, it does not alter the
482 dynamic range of spiking in pyramidal cells, which is important to encode functional information
483 under normal conditions.

484

485 **Conclusion**

486 Here, we presented data strongly arguing that MGE transplant-derived interneurons make
487 functionally inhibitory connections with host neurons. Although interneuron complexity presents
488 a potential problem for cell-based therapies, we showed that MGE-derived progenitors share the
489 same developmental lineage, innervation preference, and subtype-specific synaptic
490 characteristics as endogenous MGE-derived interneurons. This information not only suggests a
491 working mechanism underlying the functional impact of MGE progenitor transplantation but
492 also sheds light on their ability to form appropriate local connections in an established network.

493 **References**

494

495 Alvarez-Dolado M, Calcagnotto ME, Karkar KM, Southwell DG, Jones-Davis DM, Estrada RC,
496 Rubenstein JLR, Alvarez-Buylla A, Baraban SC (2006) Cortical inhibition modified by
497 embryonic neural precursors grafted into the postnatal brain. *J Neurosci* 26:7380–7389

498 Anderson SA, Eisenstat DD, Shi L, Rubenstein JL (1997) Interneuron migration from basal
499 forebrain to neocortex: dependence on *Dlx* genes. *Science* 278:474–476

500 Baraban SC, Southwell DG, Estrada RC, Jones DL, Sebe JY, Alfaro-Cervello C, García-
501 Verdugo JM, Rubenstein JLR, Alvarez-Buylla A (2009) Reduction of seizures by transplantation
502 of cortical GABAergic interneuron precursors into Kv1.1 mutant mice. *Proc Natl Acad Sci USA*
503 106:15472–15477.

504 Bezaire MJ, Soltesz I (2013) Quantitative assessment of CA1 local circuits: Knowledge base for
505 interneuron-pyramidal cell connectivity. *Hippocampus* 23:751–785

506 Butt SJB, Fuccillo M, Nery S, Noctor S, Kriegstein A, Corbin JG, Fishell G (2005) The temporal
507 and spatial origins of cortical interneurons predict their physiological subtype. *Neuron* 48:591–
508 604.

509 Calcagnotto ME, Paredes MF, Tihan T, Barbaro NM, Baraban SC (2005) Dysfunction of
510 Synaptic Inhibition in Epilepsy Associated with Focal Cortical Dysplasia. *J Neurosci* 25:9649–
511 9657

- 512 Calcagnotto ME, Zipancic I, Piquer-Gil M, Mello LE, Álvarez-Dolado M (2010) Grafting of
- 513 GABAergic precursors rescues deficits in hippocampal inhibition. *Epilepsia* 51:66–70.
- 514 Cobos I, Calcagnotto ME, Vilaythong AJ, Thwin MT, Noebels JL, Baraban SC, Rubenstein JLR
- 515 (2005) Mice lacking *Dlx1* show subtype-specific loss of interneurons, reduced inhibition and
- 516 epilepsy. *Nat Neurosci* 8:1059–1068
- 517 Davis MFF, Figueroa Velez DXX, Guevarra RPP, Yang MCC, Habeeb M, Carathedathu MCC,
- 518 Gandhi SPP (2015) Inhibitory Neuron Transplantation into Adult Visual Cortex Creates a New
- 519 Critical Period that Rescues Impaired Vision. *Neuron* 86:1055–1066
- 520 Du T, Xu Q, Ocbina PJ, Anderson S a (2008) *NKX2.1* specifies cortical interneuron fate by
- 521 activating *Lhx6*. *Development* 135:1559–1567
- 522 Elfant D, Pál BZ, Emptage N, Capogna M (2008) Specific inhibitory synapses shift the balance
- 523 from feedforward to feedback inhibition of hippocampal CA1 pyramidal cells. *Eur J Neurosci*
- 524 27:104–113
- 525 Fogarty M, Grist M, Gelman D, Marín O, Pachnis V, Kessaris N (2007) Spatial genetic
- 526 patterning of the embryonic neuroepithelium generates GABAergic interneuron diversity in the
- 527 adult cortex. *J Neurosci* 27:10935–10946
- 528 Hammad M, Schmidt SL, Zhang X, Bray R, Frohlich F, Ghashghaei HT (2015) Transplantation
- 529 of GABAergic Interneurons into the Neonatal Primary Visual Cortex Reduces Absence Seizures
- 530 in Stargazer Mice. *Cereb Cortex* 25:2970–2979

- 531 Howard MA, Baraban SC (2016) Synaptic integration of transplanted interneuron progenitor
532 cells into native cortical networks. *J Neurophysiol* 116:472–478
- 533 Howard MA, Rubenstein JLR, Baraban SC (2014) Bidirectional homeostatic plasticity induced
534 by interneuron cell death and transplantation in vivo. *Proc Natl Acad Sci U S A* 111:492–497
- 535 Hunt RF, Baraban SC (2015) Interneuron Transplantation as a Treatment for Epilepsy. *Cold*
536 *Spring Harb Perspect Med* 5:a022376
- 537 Hunt RF, Girskis KM, Rubenstein JL, Alvarez-Buylla A, Baraban SC (2013) GABA progenitors
538 grafted into the adult epileptic brain control seizures and abnormal behavior. *Nat Neurosci*
539 16:692–697
- 540 Kepecs A, Fishell G (2014) Interneuron cell types are fit to function. *Nature* 505:318–326
- 541 Lee S, Kruglikov I, Huang ZJ, Fishell G, Rudy B (2013) A disinhibitory circuit mediates motor
542 integration in the somatosensory cortex. *Nat Neurosci* 16:1662–1670
- 543 Lovett-Barron M, Turi GF, Kaifosh P, Lee PH, Bolze F, Sun X-H, Nicoud J-F, Zemelman B V,
544 Sternson SM, Losonczy A (2012) Regulation of neuronal input transformations by tunable
545 dendritic inhibition. *Nat Neurosci* 15:423–430, S1-3
- 546 Miyoshi G, Hjerling-leffler J, Karayannis T, Sousa VH, Butt JB, Battiste J, Johnson JE, Machold
547 RP, Fishell G (2010) Genetic fate mapping reveals that the caudal ganglionic eminence produces
548 a large and diverse population of superficial cortical interneurons. *J Neurosci* 30:1582–1594.

- 549 Murayama M, Pérez-Garci E, Nevian T, Bock T, Senn W, Larkum ME (2009) Dendritic
550 encoding of sensory stimuli controlled by deep cortical interneurons. *Nature* 457:1137–1141
- 551 Nery S, Fishell G, Corbin JG (2002) The caudal ganglionic eminence is a source of distinct
552 cortical and subcortical cell populations. *Nat Neurosci* 5:1279–1287
- 553 Perez SM, Lodge DJ (2013) Hippocampal interneuron transplants reverse aberrant dopamine
554 system function and behavior in a rodent model of schizophrenia. *Mol Psychiatry*, London
555 18:1193–1198
- 556 Pfeffer CK, Xue M, He M, Huang ZJ, Scanziani M (2013) Inhibition of inhibition in visual
557 cortex: the logic of connections between molecularly distinct interneurons. *Nat Neurosci*
558 16:1068–1076
- 559 Prince DA, Wilder BJ (1967) Control mechanisms in cortical epileptogenic foci. “Surround”
560 inhibition. *Arch Neurol* 16:194–202
- 561 Sebe JY, Looke-Stewart E, Dinday MT, Alvarez-Buylla A, Baraban SC (2014) Neocortical
562 integration of transplanted GABA progenitor cells from wild type and GABAB receptor
563 knockout mouse donors. *Neurosci Lett* 561:52–57
- 564 Sebe JY, Looke-Stewart E, Baraban SC (2014) GABAB receptors in maintenance of neocortical
565 circuit function. *Exp Neurol* 261:163–170
- 566 Silver RA (2010) Neuronal arithmetic. *Nat Rev Neurosci* 11:474–489

- 567 Southwell DG, Nicholas CR, Basbaum AI, Stryker MP, Kriegstein AR, Rubenstein JL, Alvarez-
 568 Buylla A (2014) Interneurons from embryonic development to cell-based therapy. *Science*
 569 344:1240622
- 570 Southwell DG, Froemke RC, Alvarez-Buylla A, Stryker MP, Gandhi SP (2010) Cortical
 571 plasticity induced by inhibitory neuron transplantation. *Science* 327:1145–1148
- 572 Tong LM, Djukic B, Arnold C, Gillespie AK, Yoon SY, Wang MM, Zhang O, Knoferle J,
 573 Rubenstein JLR, Alvarez-Buylla A, Huang Y (2014) Inhibitory interneuron progenitor
 574 transplantation restores normal learning and memory in ApoE4 knock-in mice without or with A
 575 β accumulation. *J Neurosci* 34:9506–9515
- 576 Traub RD (1983) Cellular mechanisms underlying the inhibitory surround of penicillin
 577 epileptogenic foci. *Brain Res* 261:277–284
- 578 Trevelyan AJ, Muldoon SF, Merricks EM, Racca C, Staley KJ (2015) The role of inhibition in
 579 epileptic networks. *J Clin Neurophysiol* 32:227–234
- 580 Trevelyan AJ, Watkinson O (2005) Does inhibition balance excitation in neocortex? *Prog*
 581 *Biophys Mol Biol* 87:109–143
- 582 Tricoire L, Pelkey KA, Erkkila BE, Jeffries BW, Yuan X, McBain CJ (2011) A Blueprint for the
 583 Spatiotemporal Origins of Mouse Hippocampal Interneuron Diversity. *J Neurosci* 31:10948-
 584 10970
- 585 Tyson JA, Anderson SA (2014) GABAergic interneuron transplants to study development and
 586 treat disease. *Trends Neurosci* 37:169–177

- 587 Wichterle H, Garcia-Verdugo JM, Herrera DG, Alvarez-Buylla a (1999) Young neurons from
588 medial ganglionic eminence disperse in adult and embryonic brain. *Nat Neurosci* 2:461–466.
- 589 Wichterle H, Turnbull DH, Nery S, Fishell G, Alvarez-Buylla A (2001) In utero fate mapping
590 reveals distinct migratory pathways and fates of neurons born in the mammalian basal forebrain.
591 *Development* 128:3759–3771
- 592 Xu Q, Cobos I, De La Cruz E, Rubenstein JL, Anderson SA (2004) Origins of cortical
593 interneuron subtypes. *J Neurosci* 24:2612–2622
- 594 Zhou F-W, Fortin JM, Chen H-X, Martinez-Diaz H, Chang L-J, Reynolds BA, Roper SN (2015)
595 Functional integration of human neural precursor cells in mouse cortex. *PLoS One* 10:e0120281

596 **Figure 1 Transplanted MGE cells primarily derived into PV⁺ and SST⁺ interneurons.** (A)
 597 Schematic illustration of the MGE transplantation. E13.5 MGE cells carrying ChR2-eYFP were
 598 harvested from donor mice and transplanted into P2 recipient pups. Immunostaining for ChR2-
 599 eYFP, PV and SST was performed between 28-70 DAT, and electrophysiological recordings
 600 were conducted in the CA1 regions of hippocampi between 30-70 DAT. (B) Representative
 601 labeling for ChR2-eYFP and PV in a mouse transplanted with GAD2-ChR2 MGE aged at P2+43
 602 DAT. ChR2-eYFP expression was showed in green and PV was showed in red. The image on the
 603 left shows the overview of hippocampus under 4X objective (scale bar 500 μ m). Expanded views
 604 for the boxed area were imaged under 40X objective (scale bar 200 μ m). Single-channel images
 605 for green and red are shown in the middle, and merged image is showed on the right. White
 606 arrows mark cells double-labeled. (C) Representative labeling for ChR2-eYFP and SST from the
 607 same animal as in (B). The overview of hippocampus is shown on the left (4X objective, scale
 608 bar 500 μ m). Expanded views for the boxed area are shown in the middle and on the right (40X
 609 objective, scale bar 200 μ m). White arrows mark cells double-labeled. (D) Quantitative analysis
 610 showing the percentage of interneuron subtypes in transplanted cells. PV⁺ cells comprise $28.8 \pm$
 611 1.9% ($n = 6$) of the transplanted MGE cells, whereas SST⁺ cells account for $36.3 \pm 1.9\%$ ($n = 6$).
 612 We also quantified the ratios for nNOS- ($9.4 \pm 1.6\%$), reelin- ($10.7 \pm 1.8\%$), CR- (calretinin, 5.4
 613 $\pm 1.5\%$), and VIP-positive ($0.25 \pm 0.25\%$) cells ($n = 4-5$ animals).

614 **Figure 2 Transplanted MGE-derived interneurons increase spontaneous IPSC frequency in**
615 **the hippocampus.** (A) Representative electrophysiological recordings showing spontaneous
616 IPSC activities. Recordings were all done in the stratum pyramidale of CA1. The frequency of
617 IPSC recorded from a non-transplanted mouse, NT, is 14.8 Hz (top trace), whereas that from a
618 transplanted mouse is 22.5 Hz (bottom trace). The middle trace was recorded from a pyramidal
619 cell in transplanted mouse that received no inputs from exogenous interneurons. The lack of
620 connection was verified by optogenetically activating all nearby ChR2-expressing interneurons.
621 This cell serves here as an internal control and referred to as Trans-Ctrl. The spontaneous IPSC
622 frequency of it is 12.6 Hz. (B) Quantitative comparison in the spontaneous IPSC frequency. The
623 average frequencies are 9.9 ± 0.9 (n=11), 9.8 ± 1.7 (n=12), and 15.7 ± 1.5 (n=21) Hz for NT, Trans-
624 Ctrl, and Transplanted respectively. The frequency for Transplanted is significantly higher than
625 those for the other two (one-way ANOVA, $F=5.541$ $p=0.007$ followed by Tukey post hoc
626 $p=0.029$ and 0.019 for NT versus Transplanted and Trans-Ctrl versus Transplanted
627 respectively.). There is no difference between NT and Trans-Ctrl (Tukey post hoc $p=0.997$).

628 **Figure 3 Activation of transplanted cells evokes consistent IPSC responses in native**
629 **pyramidal cells but not native interneurons.** (A) Electrophysiological traces obtained from a
630 transplanted ChR2-expressing cell. A brief 10-ms blue-light pulse elicited an action potential
631 (left trace) that was insensitive to the subsequent addition of 100 μ M gabazine (right trace).
632 Application of green-light pulses to the same cell failed to bring this interneuron over threshold
633 (middle trace). Recordings from three other transplanted cells show the same result (not shown).
634 (B) Traces recorded from a native pyramidal cell in the vicinity of transplanted interneurons.
635 While brief blue-light pulses consistently evoked IPSC responses (left traces), green-light pulses
636 failed to do the same (middle traces). Subsequent application of 100 μ M gabazine to the same
637 cell compromised blue-light pulses and blocked the generation of IPSCs (right traces). Traces for
638 single trials are shown in grey and the averaged response of the cell is showed in black. We
639 recorded a total of 11 cells and all showed consistent responses to blue light. (C) Recordings
640 obtained from native interneurons. Blue-light pulses did not generate consistent IPSCs in 15 out
641 of 16 native interneurons. Recordings from one of these six cells are shown on the left. Only 1 of
642 the 16 interneurons recorded showed small light-dependent responses (right traces). They were
643 drastically smaller and slower compared to blue-light responses shown in pyramidal cells (see
644 also text in the Results).

645 **Figure 4 Transplanted and native PV⁺ interneurons generate IPSCs with comparable**
 646 **rising kinetics.** (A) Representative recordings from a native pyramidal cell in a mouse
 647 expressing ChR2-eYFP in all the PV⁺ interneurons. Blue-light pulses evoked fast and significant
 648 IPSC responses consistently. Traces for single trials are shown in grey and the averaged response
 649 is presented in black. The amplitude of the averaged IPSC for this cell is 1683.4 pA. Recordings
 650 from nine other cells also showed consistently light-dependent IPSCs that ranged from 204.8 to
 651 1817.1 pA. (B) Recordings from a native pyramidal cell in a Parv-ChR2 MGE transplanted
 652 mouse. Traces for single trials are shown in grey and the averaged response is presented in red.
 653 Blue-light pulses evoked consistent and fast IPSCs with averaged amplitude of 78.8 pA (left
 654 traces), whereas green-light pulses failed to do so (middle traces). Applying 100 μ M gabazine to
 655 the same cell blocked all IPSC activities, either light dependent or independent (right traces). We
 656 recorded eleven other native pyramidal cells, and all of them showed the same result. The
 657 averaged IPSC amplitude ranged from 19.1 to 181.4 pA. (C) Averaged IPSC responses to blue-
 658 light from (A) and (B) were rescaled and superimposed. The black trace (IPSC from a native
 659 PV⁺ cell, nParv) shares similar rising kinetics with the red trace (IPSC from a transplanted PV⁺
 660 cell, tParv). (D) The averaged rising tau for nParv and tParv are 1.64 ± 0.29 (n=10) and 1.51 ± 0.16
 661 (n=12) ms respectively, and they are not significantly different (two-sample *t*-test, *p*=0.678).

662 **Figure 5 Transplanted and native SST⁺ interneurons generate IPSCs with comparable**
 663 **rising kinetics.** (A) Representative recordings from a native pyramidal cell in a mouse
 664 expressing ChR2-eYFP in all the SST⁺ interneurons. Blue-light pulses evoked consistent IPSCs.
 665 Traces for single trials are in grey and the averaged response is in black, for which the amplitude
 666 is 1683.4 pA. Recordings from nine other cells also showed consistent light-dependent IPSCs
 667 (52.5 to 464.2 pA). (B) Recordings from a native pyramidal cell in a mouse transplanted with
 668 SST-ChR2 MGEs. Traces for single trials are shown in grey and the averaged response in red.
 669 Blue-light pulses evoked consistent IPSCs averaged at 78.8 pA (left traces), whereas green-light
 670 pulses failed to elicit any notable responses (middle traces). Applying 100 μ M gabazine to the
 671 same cell blocked all IPSC activities (right traces). Seven other native pyramidal cells show the
 672 same responses to light and to gabazine. The averaged IPSC amplitude recorded from them
 673 ranged from 51.7 to 187.3 pA. (C) Averaged IPSC responses to blue-light from (A) and (B) were
 674 rescaled and superimposed. The black trace (IPSC responded to a native SST⁺ cells, nSST) the
 675 red trace (IPSC responded to a transplanted SST⁺ cell, tSST) show comparable rising kinetics. (D)
 676 The averaged rising tau for nSst is 6.80 ± 0.90 ms (n=10) and that for tSST 5.71 ± 1.10 ms (n=8).
 677 They are not significantly different (two-sample *t*-test, $p=0.414$).

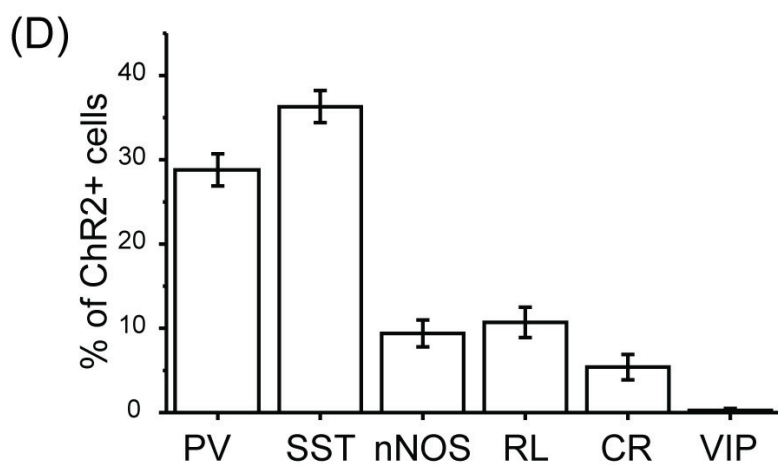
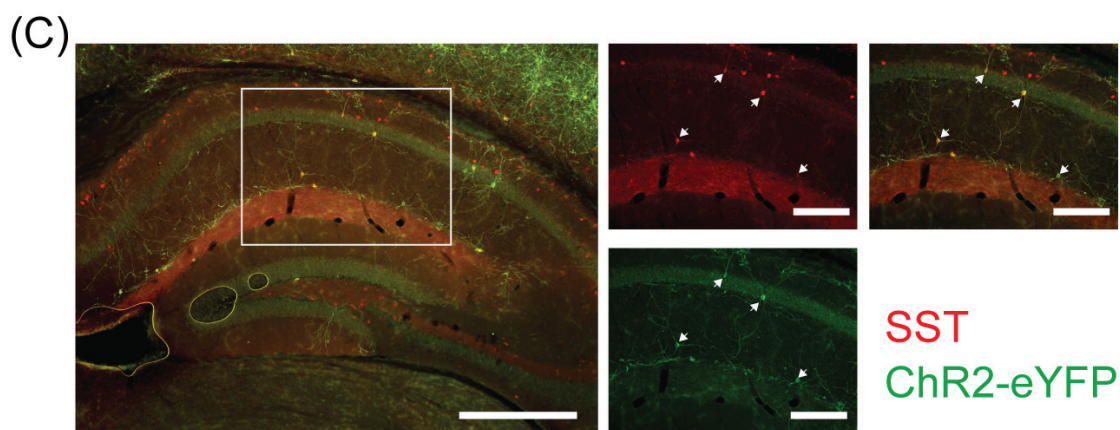
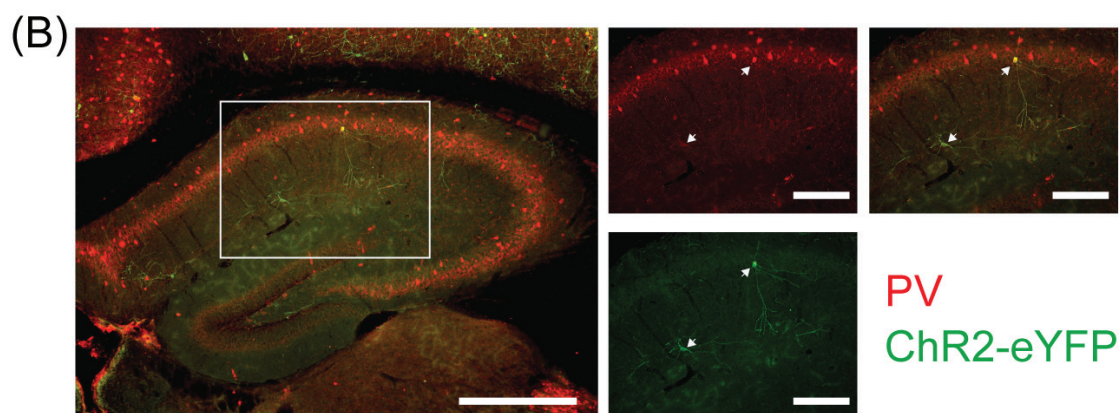
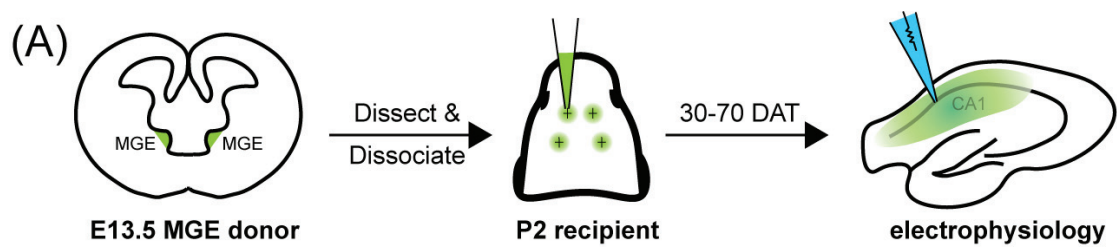
678 **Figure 6 Activation of transplanted interneurons introduce inhibitory gain control to**
 679 **native pyramidal cells.** (A) Representative traces recorded from a native pyramidal cell at
 680 various levels of current injection in the absence and presence of photostimulation. In the
 681 absence of photostimulation, 40-pA current injection (red trace) brought the cell over threshold
 682 and generated two action potentials, giving a frequency of 5 Hz. 100-pA (brown trace) and 200-
 683 pA (black trace) current injection induced higher spiking frequency at 18.7 and 29.2 Hz
 684 respectively. With simultaneous blue-light photostimulation, 40-pA was no longer sufficient to
 685 evoke action potential, and the spike frequencies induced by 100-pA and 200-pA were reduced
 686 to 15.6 and 28 Hz respectively. (B-C) I-F curves of the cell showed in (A) under various
 687 conditions. Curves were fit linearly with a data range picked manually. The slope factor of the fit
 688 line for control condition is 0.136 (open squares, $r^2=0.955$), whereas the slope factor with
 689 photostimulation is 0.138 (open circles, $r^2=0.990$). After the addition of 100 μ M gabazine, the
 690 slope factor is 0.136 (closed squares, $r^2=0.988$), and that with photostimulation is 0.135 (closed
 691 circles, $r^2=0.970$). By comparing the fit lines, we found that photostimulation right-shifts the
 692 curve by 23.7 pA, which can be reversed by the addition of gabazine. The shift in the presence of
 693 gabazine is 3.6 pA. (D) The slope factors from fit results were normalized, averaged, and
 694 compared. In the absence of gabazine, the normalized slope factor with photostimulation is
 695 1.013 ± 0.026 , which is not different from the control group (paired t -test, $n=9$, $p=0.630$). In the
 696 presence of 100 μ M gabazine, the normalized slope factor with photostimulation is 1.125 ± 0.066 ,
 697 and is not significantly different from that without photostimulation (paired t -test, $n=5$, $p=0.334$).
 698 (E) Parallel shifts in I-F curves were compared with and without gabazine. On average,
 699 activation of transplanted interneurons, tGAD2, right-shifts the I-F curve by 21.1 ± 5.5 pA, which
 700 can be rectified by 100 μ M gabazine to -2.2 ± 6.8 pA (two-sample t -test, $n=9$ and 5, $p=0.023$).

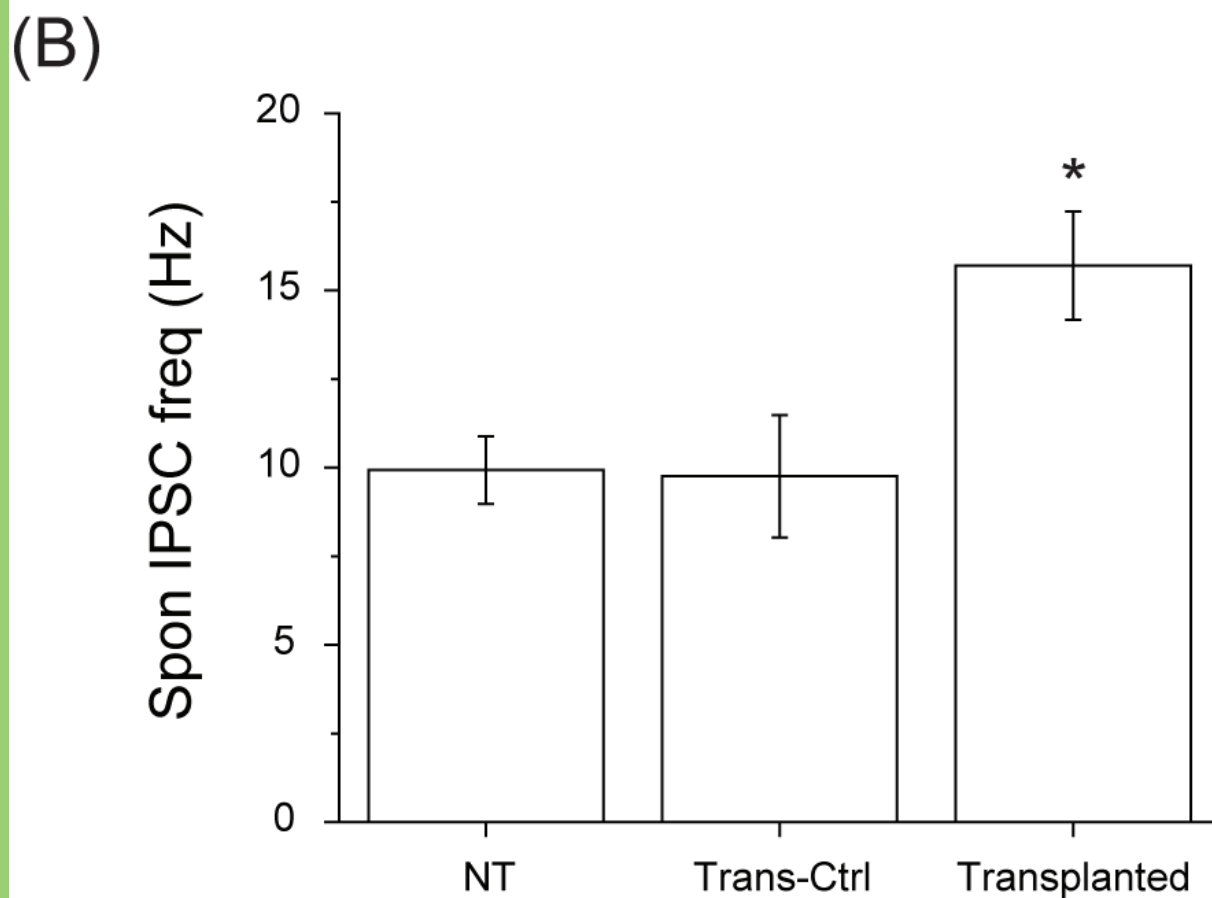
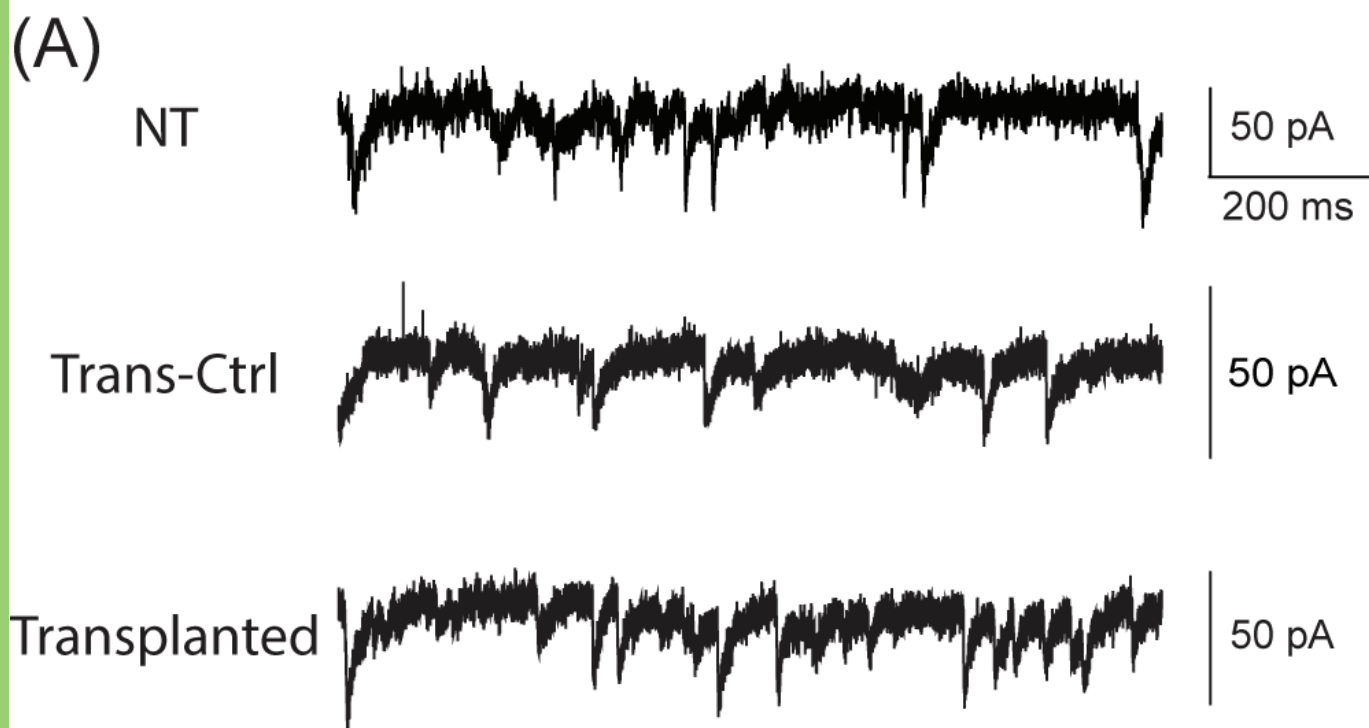
701 The minor shift in the presence of gabazine is not different from 0 (one-sample t -test, $p=0.661$).
702 Similarly, activation of native interneurons, nGAD2, shifts the I-F curves to the right
703 (342.8 ± 30.3 pA, $n=5$), and subsequent addition of 100 μ M gabazine completely eliminated the
704 effect (-5.4 ± 7.5 pA after gabazine, $n=4$; two-sample t -test, $p=0.00002$). The shift recorded in the
705 presence of gabazine is not different from 0 (one-sample t -test, $p=0.460$).

Figure 7 Transplanted PV⁺ interneurons contribute to the inhibitory gain control on native pyramidal cells. (A) Representative traces recorded from a native pyramidal cell at various levels of current injection with and without simultaneous activation of nearby transplanted PV⁺ cells. In the absence of photostimulation, 40-pA current injection elicited single action potential over a 200-ms period (red trace). When current injection was increased to 100-pA and 200-pA, the multiple spikes were elicited, and the frequencies were 19.6 (brown trace) and 37.4 (black trace) Hz respectively. In the presence of photostimulation, 40-pA current injection failed to bring the cell over threshold. Upon 100-pA and 200-pA current injection, the spike frequencies were 17.7 and 35.4 respectively. (B-C) The I-F curves under various conditions obtained from the same cells shown in (A). Linear regression was employed to fit the data. The slope factor for the control condition is 0.118 (open squares, $r^2=0.978$), and that with photostimulation is 0.110 (open circles, $r^2=0.982$). After the application of 100 μ M gabazine, the slope factors are 0.127 (closed squares, $r^2=0.972$) and 0.127 (closed circles, $r^2=0.992$) for conditions with and without photostimulation respectively. In the absence of gabazine, photostimulation shifts the I-F curve to the right by 10.6 pA, whereas it only shifts the curve by 4.4 after the addition of gabazine. (D) In the absence of gabazine, the normalized slope factor with photostimulation is 0.989 ± 0.090 and is not significantly different from that under control condition (paired t -test, $n=8$, $p=0.907$). In the presence of 100 μ M gabazine, the normalized slope factor with photostimulation is 1.013 ± 0.029 compared to that without photostimulation. There is no statistical significance between these two conditions (paired t -test, $n=6$, $p=0.399$). (E) On average, activating transplanted Parv⁺ cells shift the I-F curve of pyramidal cells by 12 ± 3.8 pA ($n=8$). This effect can be significantly reduced by 100 μ M gabazine (-2.4 ± 2.6 pA, $n=6$; two sample t -test,

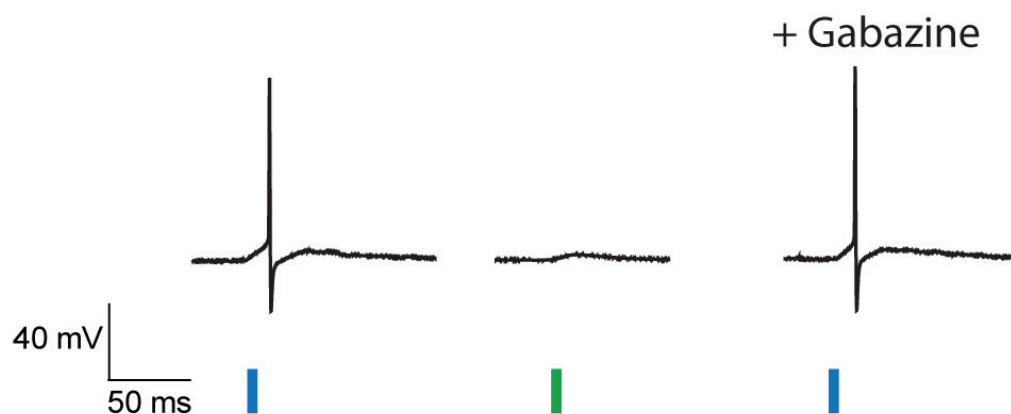
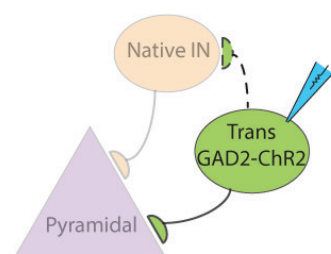
728 $p=0.013$). The shift observed in the presence of gabazine is not different from zero (one-sample
729 t -test, $n=6$, $p=0.252$).

Figure 8 Transplanted SST⁺ interneurons also contribute to the introduced inhibition on native pyramidal cells. (A) Representative traces recorded from a native pyramidal cell at various levels of current injection. Without photostimulating transplanted SST⁺ cells, 40-pA of current injection elicited a single action potential over 200 ms (red trace). The spike frequencies under 100-pA (brown trace) and 200-pA current injection (black trace) are 9 and 16 Hz respectively. With simultaneous photostimulation, 40-pA was no longer sufficient to elicit action potentials, and the frequencies evoked by 100-pA and 200-pA were reduced to 8.2 and 15.6 Hz. (B-C) The I-F curves under various conditions obtained from the same cells shown in (A). Data were fit with linear regression to obtain slope factors and intercepts along the x-axis (current axis). The slope factor for the control condition is 0.077 (open squares, $r^2=0.969$), and that with photostimulation is 0.078 (open circles, $r^2=0.946$). After 100 μ M gabazine, the slope factors are 0.065 (closed circles, $r^2=0.967$) and 0.069 (closed squares, $r^2=0.975$) for conditions with and without photostimulation respectively. In the absence of gabazine, photostimulation right-shifts the I-F curve by 9.1 pA in this cell, whereas it only shifts the curve by 4.4 after the addition of 100 μ M gabazine. (D) In the absence of gabazine, the normalized slope factor with photostimulation is 1.036 ± 0.015 and is not significantly different from that under control condition (paired t -test, $n=6$, $p=0.079$). In the presence of 100 μ M gabazine, the normalized slope factor with photostimulation is slightly lower (0.806 ± 0.103 , $n=5$) than that without photostimulation. However, this decrease is not statistically significant (paired t -test, $n=5$, $p=0.073$). (E) Photostimulating transplanted SST⁺ interneurons shifts the I-F curve of pyramidal cells by 13.3 ± 5.2 pA ($n=6$), which can be compromised by 100 μ M gabazine (-1.7 ± 2.6 pA, $n=5$; two sample t -test, $p=0.037$). The shift observed by photostimulation in gabazine is not different from zero (one-sample t -test, $n=5$, $p=0.513$).

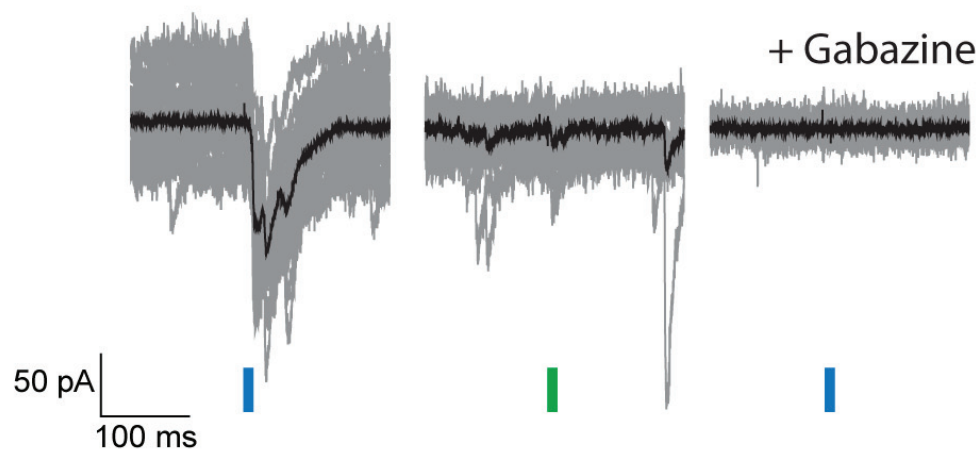
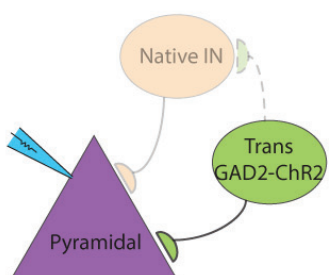




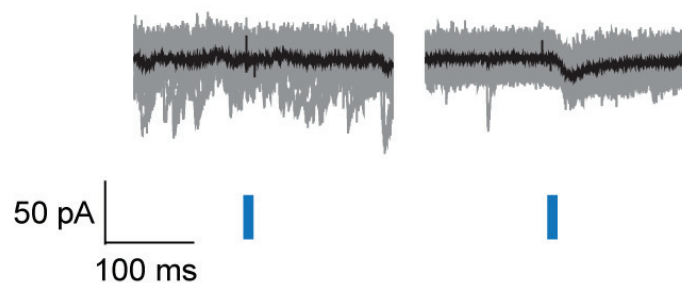
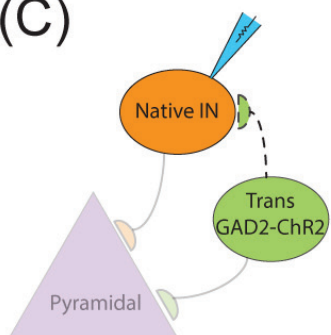
(A)

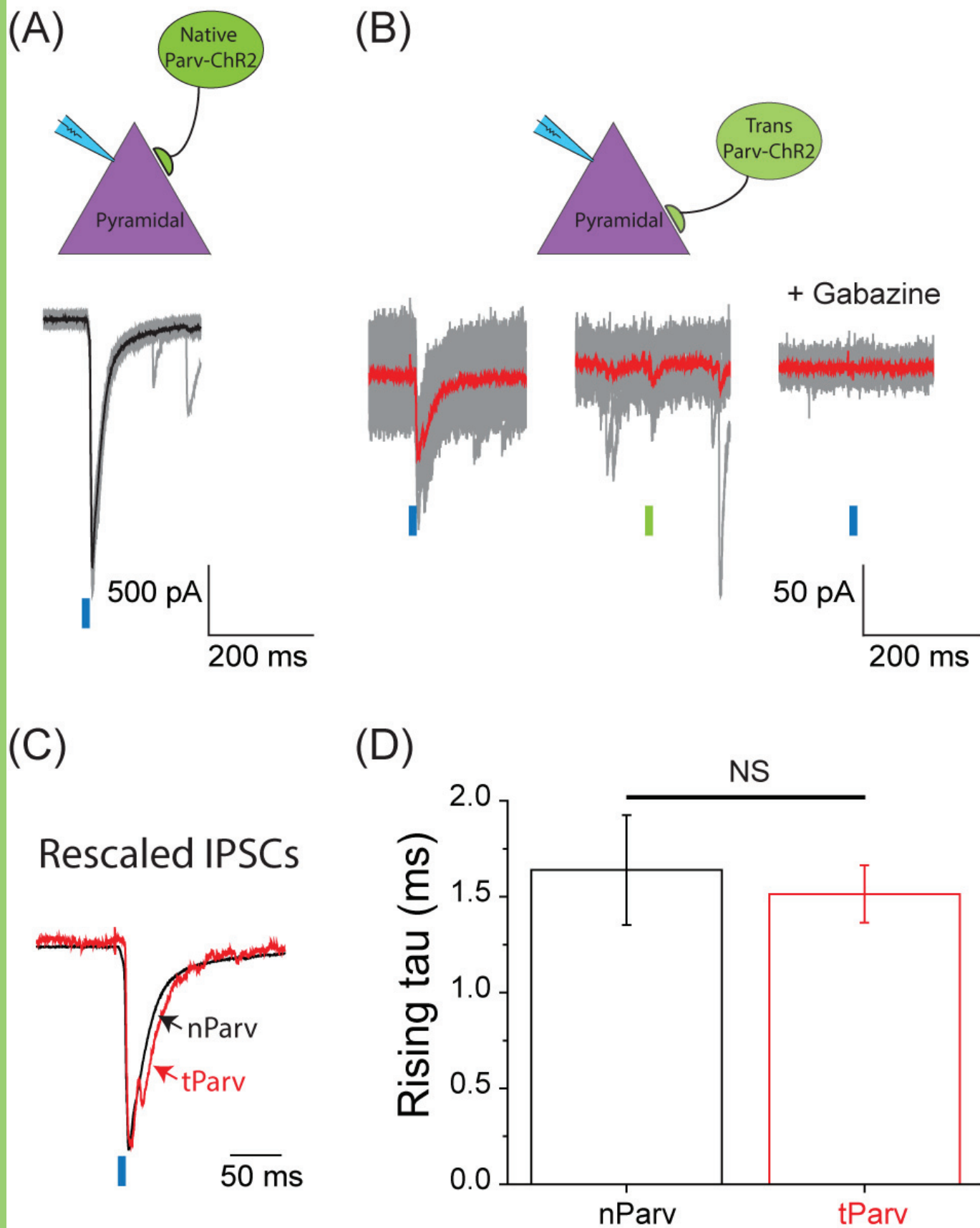


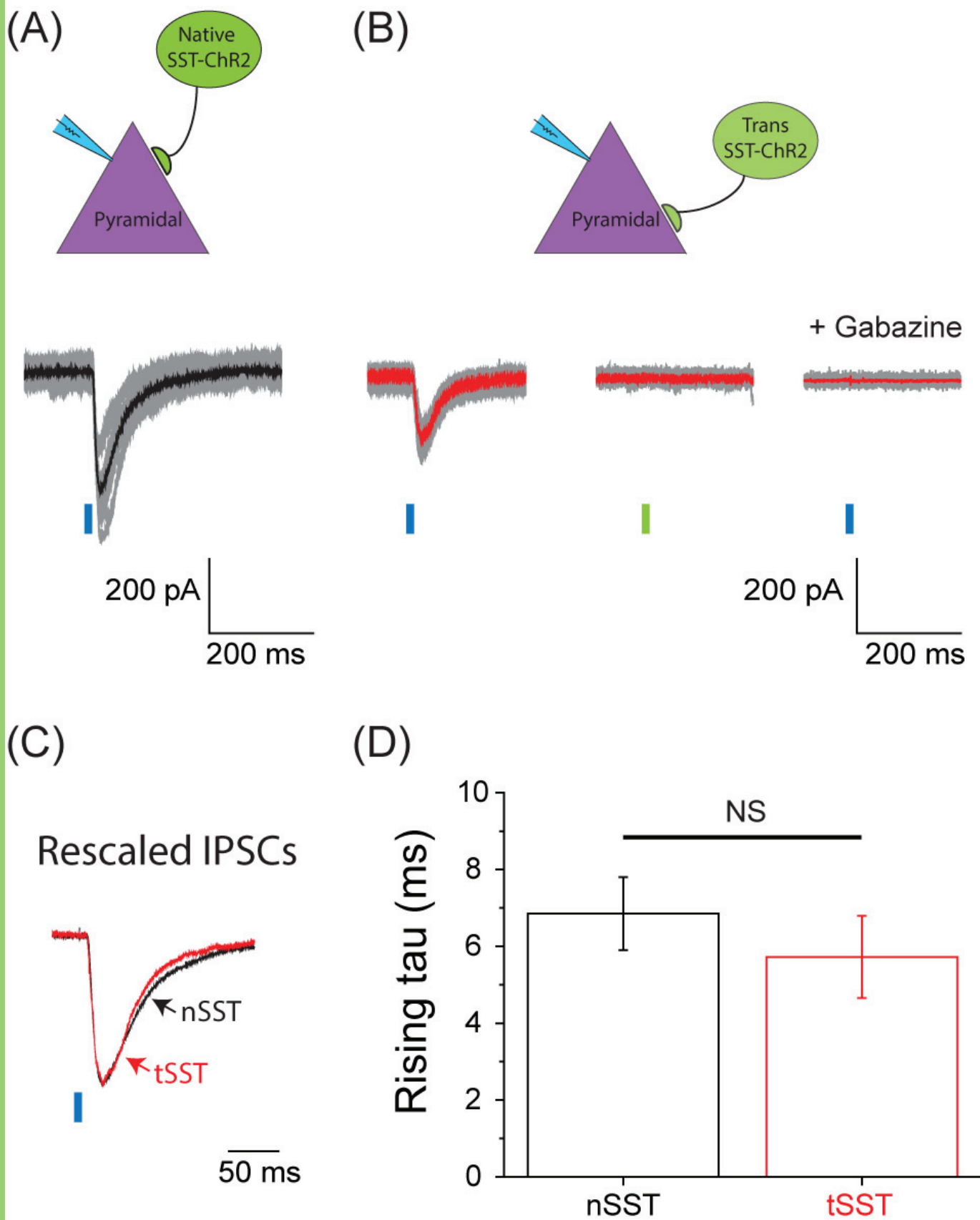
(B)

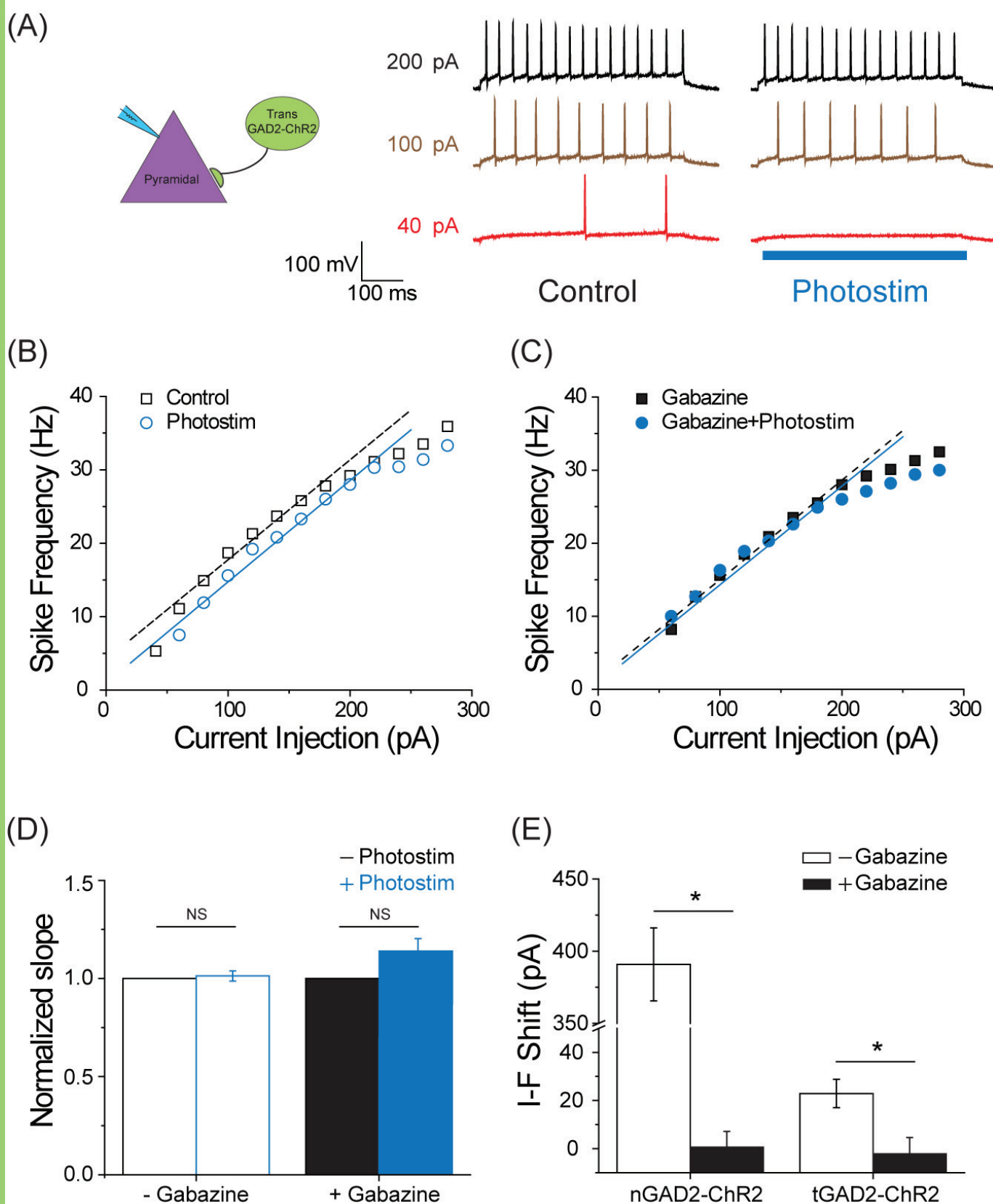


(C)

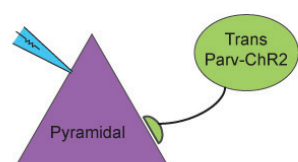




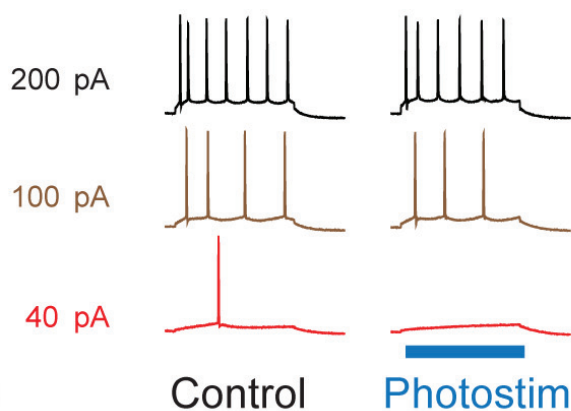




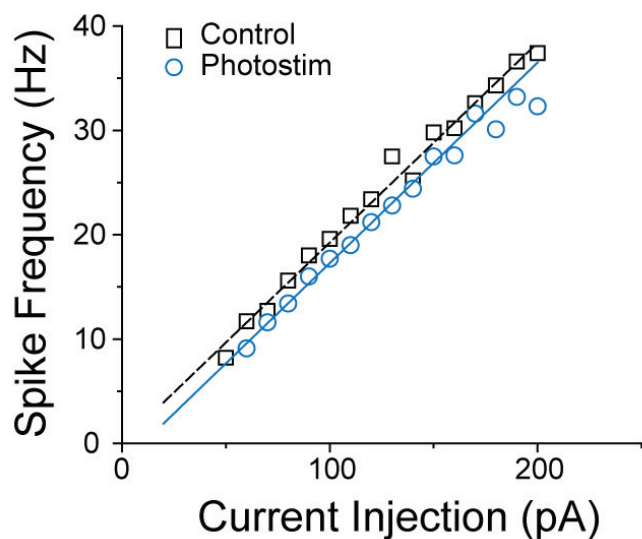
(A)



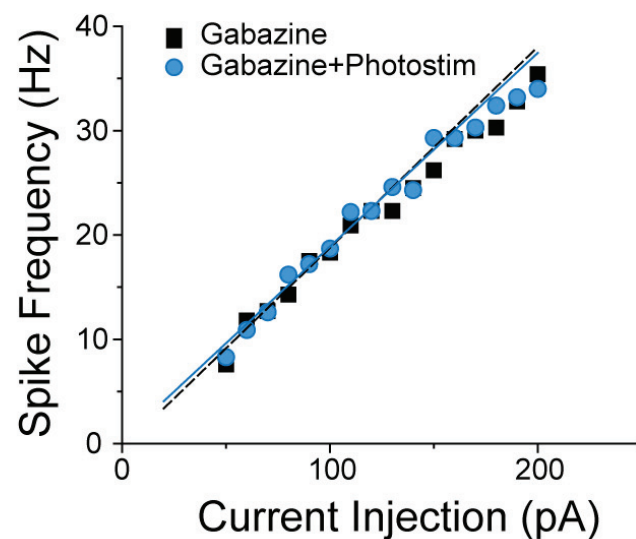
100 mV
100 ms



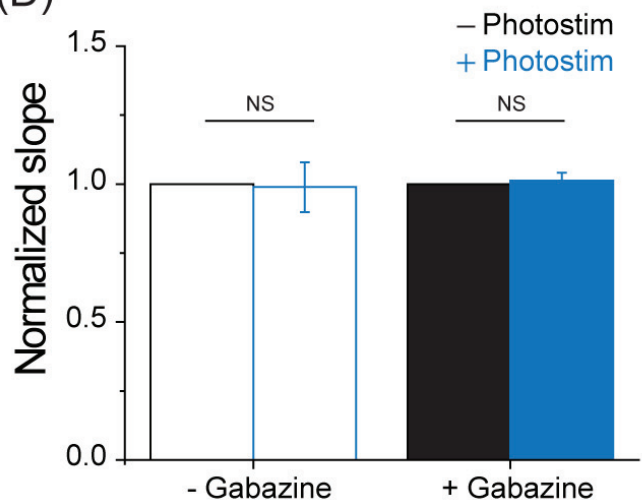
(B)



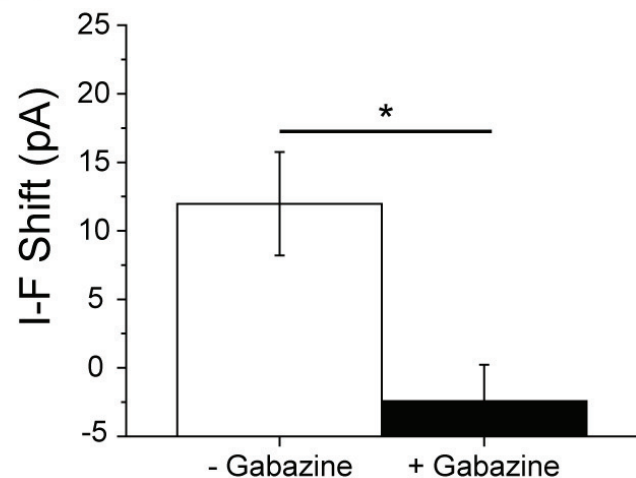
(C)



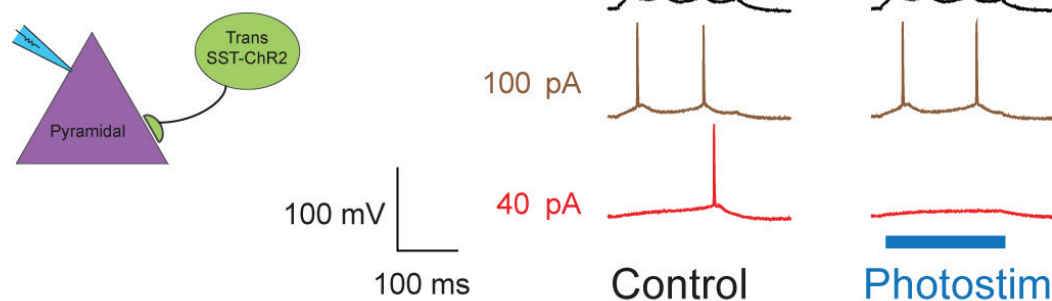
(D)



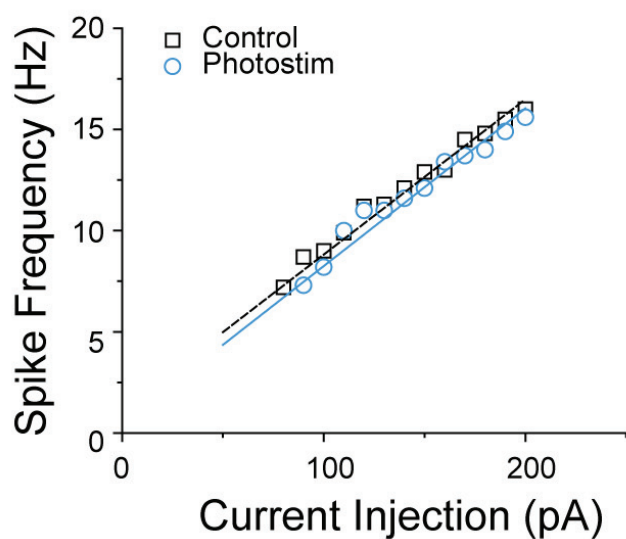
(E)



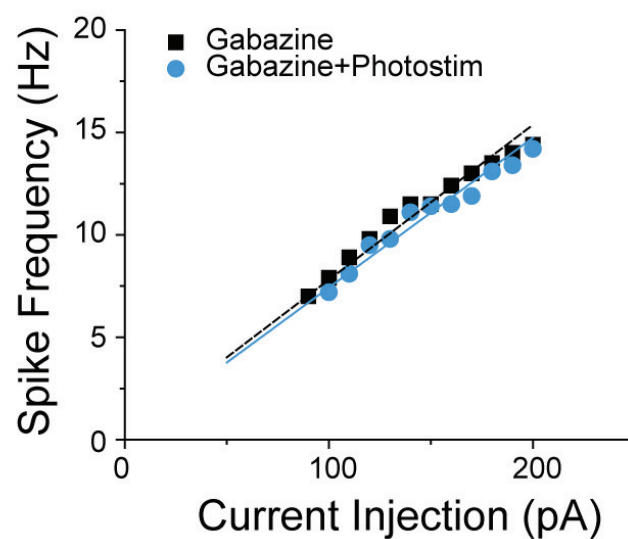
(A)



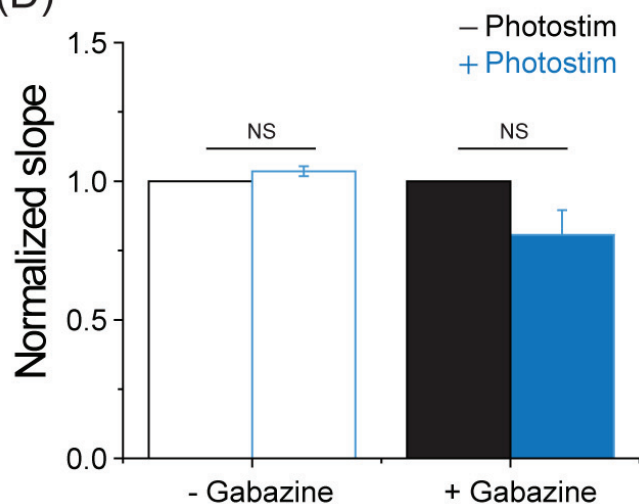
(B)



(C)



(D)



(E)

